# Post-depositional evolution over a time scale of 1 million years of eastern Mediterranean organic-rich and organic-poor sediments: new insights on the debromination and layer-silicate markers

# Evolution post-dépôt à l'échelle d'un million d'années de sédiments riches et pauvres en matière organique en Méditerranée orientale: nouveaux aperçus sur la débromination et les marqueurs argileux

Anne MURAT(1,2), Daniel BEAUFORT(3), Benoît HEBERT(3), François BAUDIN(4), Stefano BERNASCONI(5), Emmanuelle DUCASSOU(6), Céline LELIEVRE(1), Emmanuel POIZOT(1,2), Maximilien MATHIAN(3) and Olivier GRAUBY(7)

(1) Laboratoire universitaire des sciences appliquées de Cherbourg. Normandie Univ., UNICAEN, LUSAC, 50100 Cherbourg, France

(2) Conservatoire National des Arts et Métiers. INTECHMER, 50100 Cherbourg, France

(3) IC2MP UMR 7285, Université de Poitiers, 86073 Poitiers cedex 9, France

(4) iSTeP, UMR 7193, Université de Paris VI, 75005 Paris, France

(5) Geologisches Institut, ETHZ Zuerich, 8092 Zuerich, Switzerland

(6) UMR-CNRS 5805 EPOC, Université de Bordeaux, 33615 Pessac cedex, France

(7) UMR 7325 CINaM/CNRS, Université Aix-Marseille campus de Luminy, 13288 Marseille cedex 9, France

Email: anne.murat@cnam.fr

Key words: organic matter, clay minerals, bromine, eogenesis, sapropel, Mediterranean sea

Mots clés : matière organique, minéraux argileux, brome, éogenèse, sapropèle, mer Méditerranée

## Abstract

Organic matter degradation is the engine behind the biogeochemical evolution of sediments during burial. Previous research has shown that eogenesis is the seat of a complex interplay between organic matter, microbes and the most reactive part of inorganic compounds, such as clay minerals. To explore the variability and stability of bromine and clay minerals as geochemical and mineral tracers, we selected an eastern Mediterranean core that has a high degree of stability in the quality and quantity of organic matter through time at a one-million-year scale and great variability in organic matter content at a 10 ky scale. According to the very low maximal burial depth reached by these sediments (the core length is only 36.5 m), physical parameters, such as temperature and pressure, did not significantly influence the evolution of the studied parameters during the burial history. The bulk clay mineralogy of organic-rich and organic-poor sediments is similar all along the investigated core material; smectite predominates over kaolinite. The only identified authigenic minerals are biogenetic framboidal pyrite and manganese oxides. The X-ray data and the chemical compositions of the smectite are characteristic of a montmorillonite which is representative of a detrital Nile source. At a one-million-year scale, the organic matter content has no significant influence on clay eogenesis, and detrital smectite and kaolinite remain unchanged. Bromine is present in marine organic matter as organobromine compounds. During eogenesis, bromine is released from organic matter as bromide ion, resulting in an increase in the bromide concentration in the pore water with depth. Dissolved bromide can be used as a conservative tracer of the debromination of sedimentary organic matter. For the first time, we established that solid-phase BrOrg is a reliable tracer of debromination rates in marine sediments. The rate of debromination depends on the organic matter content. The rate increases from less than 2.3 x $10^{-4}$ µmolBrOrg molC$^{-1}$ y$^{-1}$ to 6.3 x $10^{-4}$ µmolBrOrg molC$^{-1}$ y$^{-1}$ when TOC varies from 0.17 to 3%. This increase is related to the development of the bacterial population and provides the basis for further investigation of other oceanic basins. For TOC values >4%, the rate of debromination decreases. We propose that the bioavailability of organic matter is another factor of variability in the debromination rate.

## Résumé

La dégradation de la matière organique est le moteur de l’évolution biogéochimique des sédiments au cours de l’enfouissement. Les recherches précédentes ont montré que l’éogenèse est le siège d’interférences complexes entre la matière organique, les microorganismes et la partie la plus réactive des composés inorganiques comme les minéraux argileux. Pour étudier la variabilité et la stabilité de traceurs géochimiques et minéralogiques, le brome et les minéraux argileux, nous avons choisi une carotte de Méditerranée orientale qui présente une grande stabilité de la qualité et de la quantité de la matière organique à l’échelle de 1 million d’années et une grande variabilité de cette quantité à une échelle de 10 ka. Considérant le faible enfouissement de ces dépôts (la carotte ne fait que 36,5 m de long), les paramètres physiques comme la température et la pression, n’influencent pas significativement l’évolution des paramètres étudiés. La minéralogie des argiles demeure semblable dans toute la carotte, que les sédiments soient riches ou pauvres en matière organique ; la smectite domine sur la kaolinite. Les seuls minéraux authigéniques identifiés sont la pyrite framboïdale biogénique et des oxydes de manganèse. Les données de diffraction de rayons X et la composition chimique de la smectite correspondent à celles d'une montmorillonite représentative des apports détritiques du Nil. A l'échelle de 1 million d'années, la quantité de matière organique n'influence pas l'éogenèse des minéraux argileux, la kaolinite et la smectite détritique demeurent inchangées. Le brome est dans la matière organique marine sous forme de composés organobromés. Pendant l'éogenèse, le brome est libéré de la matière organique sous forme d'ion bromure, il en résulte une augmentation avec l'enfouissement de la concentration en bromure dans l'eau interstitielle. Le bromure dissous peut être utilisé comme un traceur conservatif de la débromination de la matière organique sédimentaire. Pour la première fois, nous avons établi que le brome organique particulaire est un traceur valide du taux de débromination dans les sédiments marins. Le taux de débromination dépend de la quantité de matière organique. Il augmente de $2.3 \times 10^{-4}$ µmolBrOrg $molC^{-1}$ $y^{-1}$ à $6.3 \times 10^{-4}$ µmolBrOrg $molC^{-1}$ $y^{-1}$ quand le Carbone Organique Total (COT) varie de 0.17 à 3%. Cette augmentation est en relation avec le développement des populations bactériennes et fournit une base pour l'étude d'autres bassins océaniques. Pour les teneurs en COT >4%, le taux de débromination diminue. Nous proposons que la biodisponibilité de la matière organique soit un autre facteur de variabilité du taux de débromination.

# 1 Introduction

The early evolution of sediments is an important gap in the fundamental understanding of the eogenetic processes during the very shallow burial of both organic and inorganic matter [Barnes et al., 1990; McKinley et al., 2003; Worden and Morad, 2003; Worden and Burley, 2003]. The term eogenesis covers the very shallow diagenesis of both organic and inorganic matter. Eogenetic mineral reactions include the interaction of detrital mineral assemblages with pore water under the influence of a depositional system (Burley, 1993). Such reactions proceed at low temperature and are partly biochemical because they occur most often in the bacterial sulfate reduction zone (Barnes et al., 1990, Surdam et al. 1989).Organic matter degradation is the engine behind the biogeochemical evolution of sediments during burial. Field observations primarily target shallow sediment depths and fast-decaying materials, although organic matter, particularly the most refractory compounds, may degrade on geological timescales [Middelburg, 1989; Arndt et al., 2013]. Previous research showed that eogenesis is the seat of a complex interplay between organic matter, microbes and the most reactive part of the inorganic compounds, such as clay minerals. It has been established that organic matter stabilization occurs through the formation of organo-mineral complexes with layer-silicates, such as expandable clays, which are responsible for the reduction in the bioavailability of organic molecules [Mayer, 1994]. Organic matter and bacteria are known to influence the earliest reaction of non-silicates (sulfides, carbonates) and are suspected to have a role during clay eogenesis [Pryor, 1975; Coleman, 1985; Worden and Morad, 2003]. Moreover, because eogenesis is influenced by the residence time of the pore fluids, the early diagenetic assemblages are also governed by the control of sedimentation, such as climate, the rate of subsidence and the rate of sedimentation [Worden and Burley, 2003].

The aim of this study is to highlight both the organic matter and layer silicates evolution during eogenesis based on the variability or stability of bromine and clay mineral geochemical tracers.

Inorganic bromine is found as soluble bromine salts in seawater, but there are also numerous (200) known organobromine compounds that are synthesized by living organisms or formed during natural abiotic processes, such as forest fires or volcanic eruption [Gribble, 2003]. Bromine is present in marine organic matter as organobromine compounds, and a direct correlation between the bromine content and organic carbon content of sediments has been found by several authors [Price and Calvert, 1977; Pedersen and Price, 1980; Ten Haven et al., 1988; Martin et al., 1993; Ziegler et al., 2008; Leri et al. 2010]. During eogenesis, bromine is released from organic matter as bromide ion, resulting in an increase in the bromide concentration in pore water with depth [Gieskes and Mahn, 2007]. Dissolved bromide can be used as a conservative tracer of the debromination of sedimentary organic matter [Upstill-Goddard and Elderfield, 1988; Mahn and Gieskes, 2001; Berg and Solomon, 2016]. It is generally accepted that the variations in the source of organic matter, supply rate and initial solid-phase bromine concentration make the solid-phase bromine concentration an unreliable tracer for debromination in marine sediments [Berg and Solomon, 2016]. We assume that it is possible to calculate the debromination rate based on the solid-phase bromine concentration variability through time.

To achieve this objective and to explore clay mineral evolution, the studied sediment must satisfy certain requirements. The investigated site must display a high degree of stability through time of: (1) the sediment supply characteristics, (2) the sedimentation rate, which must be moderate to provide limited burial, and (3) the quality and quantity of the organic supply at one-million-year scale. However, to investigate the effect of the total organic carbon (TOC) concentration on debromination and clay mineral evolution, large variability in the organic matter content is required at a 10 ky scale.

The sediments of the eastern Mediterranean sea are good candidates to explore the evolution of organic matter during burial and over time. Organic-poor and organic-rich (sapropels) layers occur periodically in the sedimentary sequences due to a recurrent decline in deep-water ventilation. Sapropels have been the subject of many publications since the 1970s; Meyers [2006] and Rohling et al. [2015] are two of the most recent studies. This study focuses on the Neogene sediments of the Nile margin, which are situated in the far eastern Mediterranean sea, a location that enhances the sapropel layer registration in a smectite-rich sedimentary column.

## 2 Material and methods

### 2-1 Material

Core MD04 2723 (latitude 32°59.99’N, longitude 33°08.01’E, 1527 m water depth, 36.54 m long) was collected on the eastern part of the Nile continental margin during the Vanil cruise of Marion Dufresne II in 2004 (Fig. 1). This margin was built by the Nile river, one of the longest rivers in the world with a summer flood regime. Several high magnitude flood periods occurred during the Quaternary, which have been correlated with the periodic intensification of monsoonal activity over the Nile headwaters [Hassan, 1981; Rossignol-Strick, 1985; Emeis et al., 2000; Kallel et al., 2000; Schilman et al., 2001]. Nile floods and/or enhanced rainfall over the basin represent significant potential sources of fresh water for the Levantine basin. This fresh water increased the density stratification of the water column and organic matter preservation, and nutrients brought in by the runoff enhanced productivity. These conditions can trigger sapropel deposition [Olausson, 1961; Rohling, 1994; Béthoux and Pierre, 1999; Cramp and O’Sullivan, 1999; Jorissen, 1999; Casford et al., 2003; Meyers, 2006; Rohling et al., 2015]. Sapropels are episodic, basin-wide organic-rich layers that characterize the Neogene sedimentary sequences of the Mediterranean Sea. The classic lithostratigraphy of the eastern Mediterranean is based on isochronous sapropel deposits, which are synchronous throughout the deep-water basins [Kroon et al., 1998; Kallel et al., 2000; Ducassou et al., 2007]. Sapropels were identified in the studied core based on the lithological characteristics and total organic carbon (TOC) content. They appear as dark greenish and oily layers, laminated or bioturbated depending on their thickness; homogenous, color-banded or composite; with a TOC of at least 1% [Murat and Got, 2000]. The studied core has a continuous and undisturbed sedimentary record of sapropelic sequences numbered from 1 for the youngest to 29 for the oldest according to the usual standard.

## 2-2 Methodology

### 2-2-1 Sampling strategy

Core scanner measurements were conducted on a slab collected at the surface of the archive half core. The slabs were then regularly sampled to obtain isotopic data.

Geochemical analysis (TOC, Ca and Br) and characterization of clay minerals were performed on samples from the work half core. We considered 18 sapropelic sequences of the available 28 (S1, S3, S5, S6, S7, S9, S10, S11, S12, S15, S17, S19, S21, S23, S24, S27, S28 and S29) to obtain regular information through time and conducted high-frequency sampling. “Sapropelic sequence” refers to a set of samples collected below, inside and above the sapropel itself. Each sapropelic sequence corresponds to a sedimentation period ranging from 10 to 20 ky. We added a series of non-sapropelic samples deposited between 17 and 60 ka during isotopic stages 2 to 4.

To match the data obtained from the archive slab and work half core, lithologic description was performed for both. The final lithologic synthesis was based on the archive slab half core depths. The depths of the work half core samples were recalculated when necessary.

### 2-2-2 Isotope analysis

Stable isotope measurements were carried out every 10 cm. Samples were dried at 40 °C, weighed, washed and sieved with mesh widths of 63 µm and 150 µm. Isotope measurements were made on the planktonic foraminifera *Globigerinoides ruber* var. *alba* (20 specimens per sample), which were hand-picked from the > 150 µm size fraction.

The isotopic composition of carbonate was measured according to the method described in detail in Breitenbach and Bernasconi (2011). Briefly, approximately 60-80 µg of crushed, homogenized foraminifera shells were added to 4.5 ml Exetainers, (Labco, High Wycombe, UK) and flushed with pure helium. The samples were reacted with 3-4 drops of 100% phosphoric acid at 70 °C with a Thermo Fisher GasBench device connected to a Thermo Fisher Delta V mass spectrometer. The average long-term reproducibility of the measurements based on replicated standards was ±0.06‰ for $\delta^{18}O$. The instrument was calibrated with the international standards NBS19 ($\delta^{18}O$ = -2.2‰) and NBS18 ($\delta^{18}O$ = -23.01‰). The isotope values are reported in the conventional delta notation with respect to VPDB (Vienna Pee Dee Belemnite).

The age model of MD04 2723 was established by correlation of the oxygen isotope record with the Eastern Mediterranean *G. ruber* stack of Wang et al. (2010) using the Software Analyseries (Paillard et al. 1996).

### 2-2-3 Total organic carbon

The sediment samples were freeze-dried, crushed and homogenized for geochemical analysis (total organic carbon, Ca and Br contents). For the analysis of total organic carbon, sediment samples were acidified by $H_3PO_4$ (1 M) to remove carbonates, dried on a hot plate at 40 °C, and measured by combustion in a LECO CS 300 carbon sulfur analyzer. Two or three replicates of dried and homogenized sediment (50 mg) were analyzed per sample.

### 2-2-4 Rock-Eval pyrolysis

All samples were analyzed with the Rock-Eval thermal analysis technique, using a RE6 Turbo device (Vinci Technologies). Details of the RE6 apparatus are extensively described in Behar et al. [2001]. Analyses were carried out using the operating principles for the analysis of recent marine sediments. [Baudin et al., 2015]. The RE6 technique provided measurements from the sequential pyrolysis and oxidation of approximately 40 mg of desalted crushed sample. The pyrolysis gas effluents (mainly hydrocarbons) were detected and quantified by flame ionization detection (FID), and the evolution of CO and $CO_2$ gas was quantified by infrared detection during the pyrolysis and oxidation stages. The pyrolysis was carried out from 180 °C to 650 °C in an $N_2$ atmosphere, whereas the oxidation was carried out from 300 °C to 850 °C in a laboratory air atmosphere.

The RE6 technique provides information on the quantity, type (sources) and thermal evolution state of sedimentary organic matter.

### 2-2-5 Bromine and calcium analysis on single samples

The bromine and calcium contents were analyzed by X-ray fluorescence using an xSORT instrument (Spectro Ametek). The instrument was set up on a stand, and analyses were performed with the manufacturer’s Environ-H program. Ground sediment was placed in a 15 mm diameter plastic cup with a 4 µm thick polypropylene window and was manually compacted. For each sample, four replicates were analyzed during 300 s.

For Ca, 25 eastern Mediterranean sediment samples analyzed by ICP-AES (Service d’Analyses des Roches et Minéraux, SARM - Nancy). A range of concentrations from 3 to 10% was used to calibrate the equipment. The detection limit was 50 ppm, and the replicates agree within 5%.

For Br, we used standards prepared from a Mediterranean sediment for calibration. The sediment was sieved with a mesh width of 40 µm and high purity water, freeze-dried, crushed and homogenized. Known quantities of KBr solution were added to the sediment subsamples, and the subsamples were freeze-dried, crushed and homogenized. The detection limit was 5 ppm, and the replicates agreed within 5%.

The samples were also analyzed for calcium and total bromine (BrTot). Part of the samples was then rinsed twice with ultrapure water to remove residual salt from marine pore-water evaporation. A second analysis was carried out to analyze solid-phase bromine (BrSol). Previous studies have shown that pure water removes Br only to the extent that would be expected from dried interstitial water [Harvey, 1980; Mayer et al., 1981; Mayer et al., 2007] and that insignificant organic bromine was washed away [Mayer et al., 2007].

### 2-2-6 Bromine and calcium analysis by core scanner

High-resolution geochemical elemental composition records were measured directly on the archive slab surface with an Avaatech XRF Core Scanner at the EPOC Laboratory (University of Bordeaux). After cleaning and preparation of the slab surface, three separate runs (10, 30 and 50 kV, with currents of 0.6, 1.5 and 2.0 mA, respectively) were performed every 5 mm down-core with a down-core slit size of 5 mm. Sampling time was set to 10 s at 10 kV, 15 s at 30 kV and 20 s at 50 kV. The slab surface was covered with a 4 µm thin SPEXCerti Prep Ultralene1 foil to avoid contamination of the XRF measurement unit and desiccation of the sediment. Raw data spectra were processed by the analysis of the X-ray spectra using the iterative least squares software (WIN AXIL) package from Canberra Eurisys. The elements analyzed include a broad range, from aluminum $^{13}$Al through uranium $^{92}$U (Richter et al, 2006, Tjallingii, 2007). In this paper, we focused on select elements, such as calcium (Ca) and total bromine (BrTot).

To transform core scanner relative data into quantitative results, 56 sediment samples were selected within areas of the core scanner signal stability (at least 2 cm). Despite uncertainty linked to the variability of the water content, significant correlations were highlighted between the core scanner data on wet sediment samples and the X-ray fluorescence results on dried sediment samples (BrTot, r = 0.95; Ca, r = 0.93).

### 2-2-7 Characterization of clay minerals

Sediments were gently crushed, and part of the collected powder (grain size less than 50 µm) was added to deionized water to form mineral suspensions, which were dispersed ultrasonically for 2 minutes. The less than 2 µm fraction size of the sediments was collected by sedimentation, and clay minerals were characterized from the XRD patterns of the oriented preparations acquired in air-dried conditions and after ethylene glycol solvation. XRD analyses were performed using a Bruker® D8 XRD diffractometer (CuKα radiation). Diffracted beam Cu$K\alpha^{1+2}$ radiation was used (40 kV, 40 mA) and collected by a linxeye detector. Relative humidity was not controlled during data acquisition. The oriented preparation of the less than 2 µm fraction size was analyzed from 2º to 30º 2θ for a detailed characterization of the d00□ reflections of phyllosilicates.

Petrographic studies were performed on the rock fragments using a JEOL 5600 LV SEM equipped with an EDS (BRUKER XFlash 4030 Silicon drift detector). SEM observations were performed in secondary electron imaging mode (SEI) for morphological investigations and backscattering electron mode (BSE) on carbon-coated thin sections for imaging of the chemical contrast and selection of local sites for punctual chemical analysis. The analytical conditions were 15 kV, 1 nA, a counting time of 60 s and a working distance of 16.5 mm. The standards used for EDS consisted of albite (Na, Al, Si), almandine (Mg, Fe), diopside (Ca), orthoclase (K) and spessartite (Mn). Matrix corrections were performed using an integrated program (a PhiRhoz correction). The reproducibility of the standard analyses was nearly 1.5% for all of the elements, except Na, which had a reproducibility of 3%.

TEM-EDX microanalyses were conducted on individual particles deposited on a C-coated copper grid using a JEOL JEM 2011 TEM fitted with an X-Flash Silicon Drift Detector 5030 (Bruker). The data collection parameters were set as follows: magnification of 50000 x, 4 L spot size, angular tilt of 20° toward the detector, time constant of 60 kcp.s$^{-1}$, energy range of 40 keV, and corrected counting time of 30 s. The beam diameter was set to ~20 nm to reach the smallest particles.

The mid-infrared (MIR) spectra (400 to 4000 cm$^{-1}$) were acquired on KBr pellets using a Nicolet 760 FTIR spectrometer equipped with a potassium bromide (KBr) beamsplitter and a DTGS-KBr detector. The resolution was set to 4 cm$^{-1}$, with a co-addition of 100 scans. KBr pellets contained 1 mg of sample for every 150 mg of KBr powder, which was crushed into a mortar and pressed under 8 tons for 5 minutes in a hydraulic press before drying at 120 °C.

### 2-2-8 Quantification of the relative amounts of kaolinite and smectite

The relative amounts of kaolinite and smectite (smectite/kaolinite ratio) of the natural samples were obtained from normalized near infrared spectra according to the methodology described by Hébert et al. [2015]. Near-infrared spectra were collected in reflectance mode using a Nicolet 750 FTIR spectrometer with an integration sphere accessory. The spectrometer was equipped with a white light source, a $CaF_2$ beam splitter and a PbSe detector. Spectra over the 10000-4000 $cm^{-1}$ wavenumber range were obtained by co-addition of 100 spectra with 4 $cm^{-1}$ resolution. For measurements, a few hundreds of milligrams of samples were either placed directly onto the integration sphere’s shutter or disposed into IR-transparent flasks when unconsolidated.

Kaolinite and smectite have several atomic bonds within their crystal structure that absorb radiation in the near-infrared domain. The absorption bands of kaolinite and smectite can be observed in two regions of the infrared spectrum: from 1350 to 1500 nm (for overtones of OH stretching vibrations) and from 2100 to 2400 nm (for the combination of OH stretching and bending vibrations). The absorption bands of kaolinite and smectite overlap in the two regions of interest. However, kaolinite has a diagnostic absorption feature at 2165 nm, and the relative proportions of smectite and kaolinite can be determined by deconvolution of the four infrared (IR) bands that are overlapped in the region between 2100 nm and 2300 nm (Hébert et al., 2015). The smectite/smectite+kaolinite ratio calculated using this method corresponds to the percentage of smectite in the clay material, which will be referred to as Sm% hereafter.

### 2-2-9 Statistical analysis

Because each variable in the datasets used here can contain error [Laws and Archie, 1981; Sokal and Rohlf, 2012], we applied Model II regression to determine the correlations between the studied variables. This model prevents underestimation of the regression slope [Riker, 1973]. Regression analysis was performed using the lmodel2 package from R language (R Development Core Team, 2013). The statistical level of significance was defined at $p<0.05$ (Spearman’s rank correlation test).

## 3 Results

### 3-1 Sediment characteristics

The stratigraphic framework was established based on the $\delta^{18}O$ isotopic record (Fig. 2). The core displays a complete record of the last 1080 ky. According to the very low maximal burial depth reached by these sediments (the core length is only 36.5 m), physical parameters, such as temperature and pressure, did not significantly influence the evolution of the studied parameters during the burial history.

Deposits are characterized by cyclic sedimentation of organic-rich sapropel layers and organic-poor hemipelagic to pelagic sediments. Based on the sediment thickness, and without considering the upper sediment column (0-6.5 m), which was stretched by coring, the sedimentation rate varies slightly between 3.5 cm ky$^{-1}$ (6.5-20.0 m) and 2.8 cm ky$^{-1}$ (20.0-36.5 m). The Ca concentration varies from 3.2 to 22.4%, which corresponds to a carbonate content of 8 to 56% (Fig. 2). The upper part of the core (0-493 ka) displays slightly higher values, with a mean of 11.9%, than the lower part (493-1084 ka), with a mean of 10.5%. Thus, the Ca content exhibits a weak but significant anticorrelation with age (N=7250, r=-0.23).

According to the discrete occurrence of sapropels in the sedimentary column, the organic carbon content has high variability (0.17 to 6.74%, S5 sequence for example) on a small scale (10 to 20 ky) but is stable on a 1 my scale (Fig. 2). Correlation tests prove that the TOC and age are independent variables (N=323, r=-0.08). The quantity of organic matter is constant through time.

Rock-Eval pyrolysis was originally developed to characterize the organic matter present in oil source rocks [Espitalié et al., 1977], which are typically more thermally mature and at higher concentrations than thermally immature marine sediments, like the Mediterranean sapropels. Rock-Eval analyses have proved valuable in helping to determine organic matter sources and the state of diagenetic transformation in immature sediment samples [Bouloubassi et al., 1999; Baudin et al., 2007; Tribovillard et al., 2008; Hatcher et al., 2014]. The hydrogen (HI) and oxygen indexes (OI) are related to the atomic composition of the total organic matter and are commonly plotted against each other in a modified van Krevelen-type plot (Fig. 3), in which three main types of organic matter and their thermal alteration routes are defined [Tissot and Welte, 1984].

The oxidation of organic matter affects both the HI and OI. As marine organic matter (Type II) is oxidized, there is a shift to lower HI and higher OI, and the HI-OI plot approaches the characteristics of Type III vascular plant organic matter [Bouloubassi et al., 1999 on the eastern Mediterranean ODP site 969]. The results of the Rock-Eval analyses of sapropels from MD04 2723 exhibit a similar trend (Fig. 3). High organic carbon sapropel samples correspond to marine Type II organic matter that is well preserved and lower organic carbon to mainly altered marine organic matter. Microbial alteration of the organic matter during sinking or in the upper sediment layers, particularly by sulfate-reducing bacteria, has been reported to reduce the HI

[Vetö et al., 1994]. The significant positive correlation between HI and TOC supports this interpretation (N=20, r=0.89).

### 3-2 Bromine

BrTot varies from 32 to 344 ppm, with a mean of 74 ppm (Fig. 2). This variability reflects the variation in the organic matter content; higher BrTot concentrations correspond to sapropel layers. Statistical analysis of the dry sediment samples shows a significant correlation (N=323, r=0.90) between BrTot and TOC. Despite this BrTot-TOC correlation, a slight but significant evolution can be shown with the age (N=7250, r=-0.22). Without the sapropel layers, the anticorrelation is weaker (N=6335, r=-0.17). BrTot decreases through time, while TOC is constant.

To further explore this debromination, particular attention is paid to solid-phase bromine (BrSol). BrSol and TOC display a highly significant relationship (N=63, r=0.92) (Fig. 4 and Tab. 1).

The intercept of the all data regression lines tend towards zero. This proves that BrSol is bromine linked to organic matter (BrOrg). This direct correlation between the bromine content and the organic carbon content of marine sediments has been demonstrated by several authors [Price et al., 1970; Price and Calvert, 1977; Pedersen and Price, 1980; Martin et al., 1993; Ziegler et al., 2008; Leri et al., 2010].

The BrOrg results are in close proximity for low TOC contents and become more scattered with increasing TOC. This dispersion can be explained by the age of the samples. The more recent sapropelic sequences exhibit higher BrOrg than the older ones at equivalent TOC concentrations. The analysis of this issue by sapropelic sequences is presented in Table 1.

The correlations are highly significant for the S1, S5, S17 and S28 sequences. The numbers of samples are too low for the S9, S10 and S12 sequences; therefore, the correlations are not statistically valid. Nevertheless, the different sequences display a consistent trend of a decreasing slope with age (Fig. 5).

However, it remains to be determined whether the organic carbon content can affect debromination. To highlight this possibility, we selected 4 data sets corresponding to different TOC ranges and examined the evolution of BrOrg through time for each of them (Fig. 6 and Tab. 2). We chose narrow ranges of TOC (0.5 to 0.8%) and, when possible, a broad range of ages.

Organic-poor samples (TOC<0.5%) do not show significant evolution through time (N=16, r=-0.17, NS), i.e., our dataset does not allow us to demonstrate a change with age. BrOrg is always low and remains almost constant.

In contrast, the 1.5-2.3% and 2.3-3% TOC ranges show significant linear correlations of BrOrg with age, i.e., the higher the TOC range, the steeper slope, and the higher correlation coefficient (Table 2).

The rate of debromination (DBrR) increases with TOC content. For a mean TOC of 0.24%, BrOrg is almost stable (it varies from <5 to 12 ppm during 1 my). DBrR cannot be calculated, but is low. For a mean TOC of 1.83%, BrOrg decreases from 68 to 40 ppm in 1 my, and DBrR = 2.3 x $10^{-4}$ µmolBrOrg $molC^{-1}$ $y^{-1}$. For a mean TOC of 2.73%, BrOrg decreases from 147 to 32 ppm in 1 my, and DBrR increases to 6.3 x $10^{-4}$ µmolBrOrg $molC^{-1}$ $y^{-1}$.

For an organic carbon content greater than 4%, the data are scarce. Only five sapropel layers reach this level of TOC, and long periods of time are without data (Fig. 2). Compared to the other ranges studied, the variability of BrOrg is greater for samples of similar TOC and age and outliers appear. The results obtained for the full range (4.0-6.5%) are comparable to those derived from the more limited ranges (4.55-4.95% and 5.4-6.4%). However, the slopes of the calculated regression lines are lower than that for the 2.3-3% TOC range, approximately -0.07. There is an unexpected decrease in the rate of debromination to approximately 2.0 x $10^{-4}$ µmolBrOrg $molC^{-1}$ $y^{-1}$.

The intercepts provide an indication of the initial quantity of BrOrg, i.e., the quantity at the time of deposit, so it is possible to calculate the initial value of BrOrg/TOC (Table 2). For the <0.5% range, the initial BrOrg/TOC (weight ratio 29 x $10^{-4}$, molar ratio 4.4 x $10^{-4}$) is in accordance with the value of the younger sample (weight ratio 30 x $10^{-4}$, molar ratio 4.5 x $10^{-4}$, for 2 ka). Likewise, for the 1.5-2.3% range, the initial BrOrg/TOC (weight ratio 37 x $10^{-4}$, molar ratio 5.6 x $10^{-4}$) is in accordance with the value of the younger sapropel (N=4, weight ratio 37.8 x $10^{-4}$, molar ratio 5.7 x $10^{-4}$ for 8 ka). For the higher TOC ranges, the youngest samples are too old for a valuable comparison. For the 2.3-3.0% range, the initial calculated BrOrg/TOC is increasing (weight ratio 54 x $10^{-4}$, molar ratio 8.1 x $10^{-4}$). However, for higher TOC (4.0-6.5% range) the initial calculated BrOrg/TOC is decreasing (weight ratio 37 x $10^{-4}$, molar ratio 5.6 x $10^{-4}$).

The solid-phase organic bromine-age relationship holds in the organic-rich sediments, whereas it fails in the organic-poor sediments

## 3-3 Clay minerals

The bulk clay mineralogy of the organic-rich and organic-poor sediments is similar all along the investigated core material. The XRD patterns obtained from the oriented mounts of the less than 2 µm fraction size of the sediments indicate that their clay material is primarily a mixture of smectite and kaolinite, with minor amounts of micas [muscovite] and subordinated chlorite. Similar clay mineralogical composition has been described on the Nile margin [Maldonado and Stanley, 1981; Stanley et al., 1998; Hamann et al., 2009]. Smectite predominates in all samples. It was identified from its broad $d_{001}$ reflection toward 15 Å in the air-dried preparation of Ca-saturated samples that expands to 17 Å and the occurrence of a harmonic $d_{002}$ reflection close to 8.5 Å after saturation with ethylene glycol (Fig. 7).

The large width at half maximum height (FWMH > 1.5°2θ) of the $d_{001}$ reflection and the very low intensity of the $d_{002}$ reflection of the smectite after ethylene glycol saturation (which makes it difficult to identify in the XRD pattern) is indicative of the low coherent scattering domain size (CSDS) of smectite crystallites. Kaolinite is characterized by typical $d_{001}$ and $d_{002}$ reflections at 7.16 Å and 3.57 Å, respectively. From a comparative study of the XRD patterns of all samples, it can be observed that the intensity ratio between the $d_{001}$ reflections of smectite and kaolinite significantly varies all along the sapropelic sequence.

SEM observations indicate that very fine-grained clay particles (less than 2 µm) are intimately mixed with calcareous micro- to nano-fossil oozes, particles of carbonaceous material and very fine-grained detrital mineral, such as micas, alkali feldspars and quartz. The authigenic minerals identified by petrographic observation consist only of spherical aggregates of octahedral pyrite (framboidal pyrite), which is very common within the organic-rich sediments (Fig. 8), and tiny crystals of manganese oxides that have been observed locally in proximity to the sapropelic horizons.

When observed after dispersion in water and sedimentation on a glass substratum (Fig. 8b), the clay particles present a typical morphology of smectite (i.e., resulting in the aggregation of thin films of clay minerals with anhedral morphology) intimately associated with more dispersed subhexagonal plates of kaolinite. HRTEM observation of the smectite tactoids indicates that they are composed of very thin crystallites, which display a very small number of stacked individual layers (less than 5) when oriented perpendicularly to c* (Fig. 8c). This is in agreement with the XRD data, which indicated the low coherent scattering domain size (CSDS) of the smectite crystallites.

The crystal-chemical characteristics of the smectite particles do not change significantly along the investigated core. Despite a relatively large range of chemical variation, which results from intimate mixing with different types of mineral impurities, the punctual analyses obtained from SEM-EDX and TEM-EDX converge toward a composition of montmorillonite (Table 3).

All structural formulas are characteristic of dioctahedral smectite with octahedral occupancy ranging from 2 to 2.1 atoms per formula unit (a.p.f.u.), in which the tetrahedral negative charge (due to substitution of Al with Si) is very low (less than 0.2). Despite the uncertainty in the partitioning of Mg between the octahedral sheet and interlayer position and the $Fe^{2+}/Fe^{3+}$ ratio within the octahedral sheet, the negative charge of the 2:1 layer is due to $Mg^{2+}$ for Al substitution. The montmorillonitic composition of the smectite of both organic-rich and organic-poor sediments is confirmed by the middle-infrared spectra of the clay material. The OH bending bands of the phyllosilicates between 820 and 915 $cm^{-1}$ agree with the dioctahedral nature of the clay minerals (kaolinite and smectite) contained in the sample [Farmer, 1974]. Both kaolinite and smectite contributed to the 912 $cm^{-1}$ band, which was attributed to an AlAl-OH vibration. The 875 and 835 $cm^{-1}$ absorption bands were attributed to $AlFe^{3+}$-OH and $AlMg^{2+}$-OH bending vibrations, respectively [Farmer, 1974, Petit and Decarreau, 1990, Petit et al., 2002]. The quantitative analysis of the relative amounts of smectite and kaolinite in the bulk samples by NIR spectrometry (Figure 9) confirms that smectite largely predominates over kaolinite all along the investigated core.

The range of variation of the percentage of smectite in the clay material (Sm%) is restricted between 62 and 97% (Fig. 2), and no clear variation can be observed in a comparison of the S/K ratios in the different compartments of the studied core. The range of variation of the Sm% determined at the scale of the sapropelic sequence is often not far from that measured at the core-scale. The smectite content variability cannot be linked to organic matter content variation, and TOC and Sm% are two relatively independent parameters (N=191, r=-0.22, highly significant). The most significant variation of Sm% observed at the core scale is an increase in the smectite-rich samples (Sm%>90) from the bottom (oldest sediments) to the top (younger sediments) of the investigated core.

## 4 Discussion

### 4-1 Debromination

There are many ways to explore debromination.

One way is BrTot high-frequency core scanner analysis (Fig. 2). Total bromine consists of dissolved bromine and solid-phase bromine. The solid-phase bromine is linked to organic matter and immobilized, but it progressively leaves the organic matter and is released as bromide into pore water. Therefore, it decreases with age. The dissolved bromine is composed of two components: (1) bromide provided by marine pore-water salt at the time of deposition and debromination and (2) organic bromine. No significant chemical uptake processes are known to act as a sink for bromide [Berg and Solomon, 2016]. Without the influence of other processes, BrTot will remain constant. However, dissolved bromine is mobile. When debromination occurs, the bromide concentration increases in the pore water more strongly in the organic-rich layers than in the organic-poor layers. As a result, bromide is firstly transported by diffusion from organic-rich to organic-poor sediment to equalize the concentrations. On a larger timescale, bromide migrates through diffusion and/or advection back toward the overlying ocean. The end result is that BrTot and its variability range decrease with age, even though the bromide/chloride ratio increases with depth [Berg and Solomon, 2016]. The MD04 2723 core scanner data exhibits this general trend, whereas TOC remains constant at the same timescale, which supports the debromination of the organic matter and the upward bromide migration.

However, BrTot and bromide/chloride ratio analysis provide a limited estimation of debromination itself. Another way to obtain more accurate values is to compare BrTot and the organic carbon content of organic-rich sediment layers. When TOC is high, BrTot is mainly composed of bromine linked to organic matter and the pore-water bromide can be neglected. The core MD04 2723 contains two highly organic-rich sapropel layers: S5 and S28 (Fig. 2). They have similar maximum TOC contents (6.7% for S5 and 6.4% for S28) and different BrTot maximum concentrations (326 ppm for S5 and 174 ppm for S28). The debromination rate can be estimated at 3.5 x $10^{-4}$ µmolBrOrg molC$^{-1}$ y$^{-1}$, in accordance with results obtained directly by the BrOrg measurements (Tab. 2).

Studying BrOrg variability is a better way to obtain accurate values of the debromination rates. There are two pathways acting simultaneously in biological systems for the production of BrOrg, biotic production in cells of macro and microalgae as a result of the enzymatically mediated reaction of $Br^-$ and abiotic production by nucleophilic substitution [Ballschmiter, 2003]. These reactions produce aliphatic and aromatic forms of organobromine [Leri et al., 2014]. During organic matter degradation, bromine can be removed from organobromine compounds through microbial metabolic or abiotic debromination processes. One metabolic pathway in the degradation of organic material is organohalide respiration. Bacteria in anoxic environments utilize reductive dehalogenase to break the carbon-halogen bond of organohalide compounds functioning as electron acceptors. The bromine is replaced by a hydrogen atom. It has been hypothesized that this metabolic pathway using reductive dehalogenase may be an important energy source for microbial communities in the deep biosphere [Futagami et al., 2009]. The energy yield of organohalide respiration in the natural environment can be several times greater, on a per mole basis, than other metabolic pathways, such as sulfate reduction and methanogenesis [Dolfing, 2003]. Bacterial groups that have the potential to use organohalide respiration as a metabolic pathway have been found to be abundant in deep subsurface marine sediments, both geographically and with depth [Futagami et al., 2009; Orcutt et al., 2011]. Less is known about organohalide fermentation, but it has been shown to be another potential energy-producing pathway for microbes in the deep biosphere [Justicia-Leon et al., 2012; Lee et al., 2012]. Based on the BrOrg concentration variability, we have demonstrated that the rates of debromination are linked to the TOC contents. They increase from less than $2.3 \times 10^{-4}$ µmolBrOrg $molC^{-1}$ $y^{-1}$ up to $6.3 \times 10^{-4}$ µmolBrOrg $molC^{-1}$ $y^{-1}$ when TOC varies from 0.17 to 3%. For higher TOC values, precise rates of debromination could not be reliably established due to scattered data (Fig. 6), but they decrease in all cases. To explore the relationship between TOC and the rate of debromination, two assumptions are proposed: the rate of debromination depends on microbial activity and/or the bioavailability of organic matter. Cragg et al. (1998) studied the bacterial concentrations at the eastern Mediterranean ODP site 969, which has similar cyclic sedimentation of organic-poor and organic-rich (80 sapropels beds to 116 mbsf) sediments. Within the range of TOC concentrations usually encountered in marine sediments (0-3%), the data set produced a significant correlation between TOC and bacterial populations, in good agreement with the general profile derived from other ODP sites. The addition of data with higher TOC destroyed the relationship, which suggests that at high concentrations, such as those found in sapropels, TOC is effectively present in excess and ceases to be a limiting factor for bacterial population size. The remarkable fact that the bacterial populations and rates of debromination both increase with the TOC concentration but only within the 0-3% range suggests that debromination is quantitatively dependent on microbial activity. However, it is difficult to explain why the TOC concentration does not behave as a limiting factor when its content is greater than 3%. Cragg et al. (1998) suggested that organic carbon within the sapropel layers must be predominantly recalcitrant and only slowly bioavailable.

The organic carbon content of the sapropel layers depends on the rate of degradation/preservation of organic matter. During sapropelic periods, the water column is stratified. The upper layer is normally oxygenated, and aerobic organic matter degradation by microorganisms occurs. The lower layer is oxygen-depleted, and organic matter is oxidized through various less-effective anaerobic pathways [Demaison and Moore, 1980; Emerson and Hedges, 1988]. We assume that very stable stratification results in a high-TOC sapropel (more than 3%), and low organic carbon sapropels correspond to instable stratification with periodic reoxygenation of the entire water column [Casford et al., 2003; Stefanelli et al., 2005 and Meyers et al., 2006; Rohling et al., 2015]. The two degradation pathways produce different organic molecules, which are less bioavailable in the case of oxygen-depleted conditions. Therefore, in organic carbon-rich sapropels (TOC > 3%) organic matter would not be as bioavailable as in low organic carbon sapropels (TOC < 3%). Furthermore, the initial BrOrg/TOC also decreases at the 3% TOC. The sediments with 2.3-3.0% TOC provide ideal conditions for the development of bacterial groups that may have the potential to use organohalide respiration: a high content in Br-rich organic matter. Sediment with higher TOC has higher BrOrg content but a lower initial BrOrg/TOC and could be less attractive.

However, some factors of the debromination rate variability for very high organic carbon content remain to be identified. We need to explain why two samples collected 3 cm apart within the same sapropel (S17) with the same TOC concentration (4.7 and 4.8%) present different BrOrg contents (140 and 86 ppm). The first cited sample follows the general debromination trend, whereas the second displays evidence of a higher rate (Fig. 6). Therefore, sometimes high rates of debromination occur, even for high organic carbon content layers. The explanation of this difference does not lie in the burial conditions, which are the same. Rather, the solution is in the initial organic matter quality, which is dependent on the production and/or degradation conditions. A 1 cm thick sample corresponds to three centuries of basin history, a duration cannot analyze the climatic variability of the temperature sea-surface, Nile floods or depth of the oxic/anoxic water interface, three parameters that may have influenced the quality of the produced and preserved organic matter [Meyers, 2006]. Sapropels are organic-rich layers, but for most of them, preserved organic matter represents a small portion of the produced organic matter. For low

TOC content sapropels (1-3%), the initially produced marine organic matter is mainly degraded. Thus, the degradation step plays a major role in the quality of the finally preserved organic matter. In contrast, for higher organic carbon sapropels, even if the degradation pathways remain important, a higher proportion of produced organic matter is preserved and the quality of the produced organic matter is a more important factor in the variability of bioavailability.

## 4-2 Clay mineral evolution

The core MD04 2723 provides an opportunity to examine the evolution of layer silicates in parallel to that of organic matter during the last million years of sedimentation and eogenesis of sediments in the eastern part of the Egyptian continental margin. Kaolinite and smectite are known to be the diagnostic clay minerals of the eogenesis of mudstones (Burley, 1993 and references therein). However, it is unclear whether these clay minerals originate from sedimentation (detrital clays) and/or from the eogenesis of the sediments during their incipient burial.

This study shows that (1) there is no evidence of authigenic clay minerals and that (2) dioctahedral smectite largely predominates over kaolinite in the samples collected all along the core MD04 2723. More specifically, infrared spectroscopy and microchemical analyses indicated that the crystal chemistry of the dioctahedral smectite agrees with that of montmorillonite. Its mineralogical and chemical composition is similar to that of the smectite previously identified in the Nile suspended matter [Dekov et al., 1997] and the Nile alluvial soils in Egypt [Kishk et al., 1976] and the range of Sm% measured all along the core is in full agreement with the published clay mineral data from the Nile assemblage [Hamann et al., 2009]. On the basis of the qualitative analysis in this study, it is assumed that the clay mineralogy of the core MD04 2723 is essentially representative of the detrital Nile source. However, on the basis of quantitative analysis, Sm% variability is likely to occur at two different timescales.

Some sapropelic sequences exhibit a wide range of variation in Sm% (S10, for example, 71-97%, Fig. 2) while others do not (S15, for example, 66-73%, Fig. 2). The highest Sm% can be located either in the organic-rich (S10 and S11 sequences) or in the organic-poor (S7 and S9 sequences) sequences. The controlling factor of the Sm% variation is not climatic because all four aforementioned sapropels correspond to low values of the $\delta^{18}O$ isotopic record. As expected from the absence of diagenetic evolution of clay minerals, the smectite concentration and TOC are not correlated.

Over a span of one million years, a slight change occurs, which is highlighted by the mean values for each sapropelic sequence (Fig. 10).

The lower part of the core (500 to 1080 ka) is characterized by a nearly constant and low (69-73%) Sm%, whereas the upper part is characterized by heterogeneous mean values with successively increasing or decreasing gradients (Sm% between 71 and 88%), which cannot be linked to the $\delta^{18}O$ isotopic record. The 500 ka limit also affects others sedimentary parameters, such as the Ca concentration and sedimentation rate. The last 500 ky shows an increase in the sedimentation rate, the carbonate content and the Sm% variability. Even though the cause of these variations remains uncertain, the hypothesis of temporal change in detrital sources can be invoked.

## 5 Conclusion

The studied site displays both a high degree of stability in the organic supply at a one-million-year scale and great variability in the organic matter preservation at a 10 ky scale, an ideal situation to highlight and discuss the influence of the organic matter content on the mineralogical and geochemical evolution during eogenesis. This allows us to demonstrate that at a one-million-year scale, the organic matter content has no significant influence on clay eogenesis. Detrital smectite and kaolinite remain unchanged everywhere, even within the sapropels where high bacterial populations are active.

We have demonstrated that solid-phase BrOrg is a reliable tracer of debromination rates in marine sediments. Based on the highly variable TOC concentration of the eastern Mediterranean sea, it was determined that the rates of debromination depend on the organic matter content. This observation provides the basis for further investigation of other oceanic basins. Within the range of TOC concentrations usually encountered in marine sediments (0-3%), both bacterial populations and the rates of debromination increase with TOC content. It can be assumed that these two parameters are correlated. The increase in bioavailable organic matter induces growth of active bacterial populations, resulting in higher rates of debromination. In the eastern Mediterranean sea, the depth profile of the bacterial populations is in good agreement with the general profile derived from other oceans [Cragg et al., 1998; Parkes et al., 2014]. This suggests that the rates of debromination obtained in the Mediterranean sea are relevant for all ocean basins. This assumption should be supported by further investigations, which could be performed on a basin that displays a high and stable organic carbon content over time. This approach would provide only one rate of debromination. It would be more interesting to search for a Mediterranean-like basin that exhibits both a high degree of stability of the organic supply at a one-million-year scale and great variability in the organic matter content at a 10 ky scale. Different rates of debromination could be investigated. Extending the time-range of the sedimentation and diagenetic evolution to a ten-million-year scale would show whether clay minerals remain stable over a one-million-year scale due to of slow reaction kinetics.

Acknowledgements

This work was funded by the French program “Action Marges”. We thank Jean Mascle and the on-board scientific team for their assistance and Yvon Balut and the Marion Dufresne II crew (French Polar Institute: IPEV) for technical support during the Vanil cruise.

References:

ARNDT S., JØRGENSEN B.B., LAROWE D.E., MIDDELBURG J.J., PANCOST R.D. & REGNIER P. (2013). - Quantifying the degradation of organic matter in marine sediments: A review and synthesis. - *Earth-Science Reviews*, **123**, 53–86

BALLSCHMITER K. (2003). - Pattern and sources of naturally produced organohalogens in the environment: biogenic formation of organohalogens. - *Chemosphere*, **52**, 313–324.

BARNES M. A., BARNES W.C. & BUSTIN R. M. (1990). - Chemistry and diagenesis of organic matter in sediments and fossil fuels. *In:* Geoscience Canada Reprint Series, Diagenesis, 189-204.

BAUDIN F., COMBOURIEU-NEBOUT N. & ZAHN R. (2007). - Signatures of rapid climatic changes in organic matter records in the western Mediterranean Sea during the last glacial period. – *Bull. Soc. Géol. Fr.*, **178**, 1, 3-13.

BAUDIN F., DISNAR J.P., ABOUSSOU A. & SAVIGNAC F. (2015). - Guidelines for Rock–Eval analysis of recent marine sediments. – *Org. Geochem.*, **86**, 71–80.

BEHAR F., BEAUMONT V. & DE PENTEADO, H.L. (2001). - Rock–Eval 6 technology: performances and developments. - *Oil and Gas Science and Technology,* **56**, 111–134.

BERG R.D. & SOLOMON E.A. (2016). - Geochemical constraints on the distribution and rates of debromination in the deep subseafloor biosphere. – *Geochim. Cosmochim. Acta*, **174**, 30–41.

BÉTHOUX J.P. & PIERRE C., (1999). - Mediterranean functioning and sapropel formation: respective influences of climate and hydrological changes in the Atlantic and the Mediterranean. - *Mar. Geol.,* **153**, 29–39.

BOULOUBASSI I., RULLKÖTTER J. & MEYERS, P.A. (1999). - Origin and transformation of organic matter in Pliocene–Pleistocene Mediterranean sapropels: organic geochemical evidence reviewed. - *Mar. Geol.,* **153**, 177–197.

BREITENBACH S.F.M. & BERNASCONI S.M. (2011). - Carbon and oxygen isotope analysis of small carbonate samples (20 to 100 µg) with a GasBench II preparation device. - *Rapid Communications in Mass Spectrometry,* **25**, 1910-1914.

BURLEY S. D. (1993). - Models of burial diagenesis for deep exploration plays in jurassic fault traps of the central and Northern North Sea. - *Geological Society, London, Petroleum Geology Conference series 1993*, **4**, 1353-1375.

CASFORD J.S.L., ROHLING E.J., ABU-ZIED R.H., JORISSEN F.J., LENG M. & THOMSON J. (2003). A dynamic concept for eastern Mediterranean circulation and oxygenation during sapropel formation. - *Palaeogeogr. Palaeoclimatol. Palaeoecol.*, **190**, 103–119.

COLEMAN M. L. (1985). - Geochemistry of non silicate minerals: kinetic considerations. - *Philosophical Transaction of the Royal Society of London*, **315**, 39-56.

CRAGG B. A., LAW K.M., CRAMP A, & PARKES R.J. (1998). - The response of bacterial populations to sapropels in deep sediments of the Eastern Mediterranean (site 969). – *In:* A.H.F Robertson, K.-C. Emeis, C. Richter, & A. Camerlenghi Eds., Proceedings of the Ocean Drilling Program, Scientific Results*,* Vol. 160, Texas A&M University, College Station, TX, 303-307.

CRAMP A. & O'SULLIVAN G. (1999). - Neogene sapropels in the Mediterranean: a review. - *Mar. Geol.,* **153**, 11–28.

DEKOV V.M., KOMY Z., ARAUJO F., VAN PUT A. & VAN GRIEKEN R. (1997). – Chemical composition of sediments, suspended matter, river water and ground water of the Nile (Aswan-Sohag traverse). – *The science of the total environment*, **201**, 195-210.

DEMAISON G.J. & MOORE G.T. (1980). - Anoxic environments and oil bed genesis. -*Am. Assoc. Pet. Geol. Bull.*, **64**, 1179–1209.

DOLFING J. (2003). - Thermodynamic Considerations for Dehalogenation. – *In*: M. M. Häggblom, I. D. Bossert Eds, Dehalogenation: Microbial Processes and Environmental Applications. Springer, 89–114.

DUCASSOU E., CAPOTONDI L., MURAT A., BERNASCONI S., MULDER T., GONTHIER E., MIGEON S., DUPRAT J., GIRAUDEAU J. & MASCLE J. (2007). -

Multiproxy late quaternary stratigraphy of the Nile deep-sea turbidite system — Towards a chronology of deep-sea terrigeneous systems. – *Sedimentary Geology,* **200**, 1–13.

EMEIS K.C., SAKAMOTO T., WEHAUSEN R. & BRUMSACK H.J. (2000). - The sapropel record of the eastern Mediterranean Sea — results of Ocean Drilling Program Leg 160. - *Palaeogeogr. Palaeoclimatol. Palaeoecol*. **158**, 371–395.

EMERSON S. & HEDGES J.I. (1988). - Processes controlling the organic carbon content of open ocean sediments. *Paleoceanography,* **3**, 621–634.

ESPITALIE J., LAPORTE J.L., MADEC M., MARQUIS F., LEPLAT P., PAULET J. & BOUTEFEU A. (1977). - Méthode rapide de caractérisation des roches mères, de leur potentiel pétrolier et de leur degré d'évolution. - *Rev. Inst. Fr. Pét*., **32**, 23–42.

FARMER V.C. (1974). - The Infrared Spectra of Minerals. - *Monograph, 4. The Mineralogical Society*, London, 539 p.

FUTAGAMI T., MORONO Y., TERADA T., KAKSONEN A. H. & INAGAKI F. (2009). - Dehalogenation activities and distribution of reductive dehalogenase homologous genes in marine subsurface sediments. - *Appl. Environ. Microbiol*., **75**, 6905–6909.

GIESKES J.M. & MAHN C. (2007). - Halide systematics in interstitial waters of ocean drilling sediment cores. - *Applied Geochemistry*, **22**, 515–533.

GRIBBLE G.W. (2003). - The diversity of naturally produced organohalogens. *Chemosphere*, **52**, 289–297.

HAMANN, Y., EHRMANN, W., SCHMIEDL, G., & KUHNT, T. (2009). - Modern and late Quaternary clay mineral distribution in the area of the SE Mediterranean Sea. - *Quaternary Research*, **71**, 453-464.

HATCHER, P., RAVIN, A., BEHAR, F., BAUDIN, F. (2014). - Diagenesis of organic matter in a 400 m organic rich sediment core from offshore Namibia using solid state 13C NMR and FTIR. – *Org. Geochem.*, **75**, 8-23.

HARVEY G.R. (1980). - A study of the chemistry of iodine and bromine in marine sediments. - *Mar. Chem.,* **8**, 327–332.

HASSAN F.A. (1981). - Historical Nile floods and their implications for climatic change. – *Science*, **212,** 5, 1142–1144.

HATCHER P., RAVIN A., BEHAR F. & BAUDIN F. (2014). - Diagenesis of organic matter in a 400 m organic rich sediment core from offshore Namibia using solid state 13C NMR and FTIR. – *Org. Geochem.*, **75**, 8-23.

HÉBERT B., BEAUFORT D., ROY R., POURADIER A. & JIKIBAYEV R. (2015) - New methods to quantify clay minerals in the uranium deposits hosted in sands of the Chu Sarysu Basin (South Kazakhstan) based on visible and near-infrared field spectrometry. *In: Proc. 13th Biennial SGA Meeting*. - Nancy, France, 587-589.

JORISSEN F.J. (1999). - Benthic foraminiferal successions across Late Quaternary Mediterraenan sapropels. - *Mar. Geol.*, **153**, 91–101.

JUSTICIA-LEON S. D., RITALAHTI K. M., MACK E. E. & LÖFFLER F. E. (2012). - Dichloromethane fermentation by a Dehalobacter sp. in an enrichment culture derived from Pristine river sediment. - *Appl. Environ. Microbiol*., **78**, 1288–1291.

KALLEL N., DUPLESSY J.-C., LABEYRIE L., FONTUGNE M., PATERNE M. & MONTACER, M. (2000). - Mediterranean pluvial periods and sapropel formation over the last 200 000 years. - *Palaeogeogr. Palaeoclimatol. Palaeoecol.*, **157**, 45–58.

KISHK F.M., EL-ATTAR H.A., HASSAN M.N. & EL-SHEEMY H. (1976). - Mineralogical and chemical composition of the clay fraction of some Nile alluvial soils in Egypt. – *Chem. Geol.*, **17**, 295-305.

KROON D., ALEXANDER I., LITTLE, M., LOURENS L.J., MATTHEWSON A., ROBERSTON A.H.F. & SAKAMOTO T. (1998). - Oxygen isotope and sapropel stratigraphy in the eastern Mediterranean during the last 3.2 million years. – *In:* Proceedings of the Ocean Drilling Program, Scientific Results, Leg 160, 181–189.

LAWS E.A. & ARCHIE J.W. (1981). – Appropriate use of regression analysis in marine biology. - *Mar.Biol.,* **65**,13–16.

LEE M., LOW A., ZEMB O., KOENIG J., MICHAELSEN A. & MANEFIELD M. (2012). - Complete chloroform dechlorination by organochlorine respiration and fermentation. - *Environ. Microbiol*., **14**, 883–894.

LERI A. C., HAKALA J. A., MARCUS M. A., LANZIROTTI A., REDDY C.M. & MYNENI S. C. B. (2010). - Natural organobromine in marine sediments: new evidence of biogeochemical Br cycling. - *Global Biogeochem. Cycles*, **24**, GB4017.

LERI A.C., MAYER L.M., THORNTON K.R. & RAVEL B. (2014). - Bromination of marine particulate organic matter through oxidative mechanisms. – *Geochim. Cosmochim. Acta*, **142**, 53–63.

MC KINLEY J.M., WORDEN R.H. & RUFFELL A.H. (2003). Smectites in Sandstones: a review of the controls on occurrence and behaviour during diagenesis. *In:* R.H. Worden & S. Morad (Eds.), Clay mineral cements in Sandstones. Blackwell Publishing, 109-128.

MAHN, C. L. & J. M. GIESKES (2001). - Halide systematics in comparison with nutrient distributions in sites 1033B and 1034B, Saanich Inlet: ODP Leg 169S. - *Mar. Geol*., **174**, 1‑4, 323‑339.

MALDONADO A. & STANLEY D. J. (1981). - Clay mineral distribution patterns as influenced by depositional processes in Southeastern Levantine Sea. - *Sedimentology*, **28**, 21-32.

MARTIN J. B., GIESKES J. M., TORRES M. & KASTNER M. (1993). - Bromine and iodine in Peru margin sediments and pore fluids: implications for fluid origins. *Geochim. Cosmochim. Acta*, **57**, 4377–4389.

MAYER L.M., MACKO S.A., MOOK W.H. & MURRAY S.M. (1981). – The distribution of bromine in coastal sediments and its use as a source indicator for organic matter. - *Org. Geochem.,* **3**, 37–42.

MAYER L.M. (1994). - Surface area control of organic carbon accumulation in continental shelf sediments. - *Geochim. Cosmochim. Acta*, **58**, 1271–1284.

MAYER L.M., SCHICK L.L., ALLISON M., RUTTENBERG K. & BENTLEY S. (2007). - Marine vs. terrigenous organic matter in Louisiana coastal sediments: the uses of Bromine: organic carbon ratios. - *Mar. Chem.*, **107**, 244–254.

MEYERS P.A. (2006). - Paleoceanographic and paleoclimatic similarities between Mediterranean sapropels and Cretaceous black shales. - *Palaeogeogr. Palaeoclimatol. Palaeoecol.,* **235**, 305–320.

MIDDELBURG J.J. (1989). - A simple rate model for organic-matter decomposition in marine-sediments. - *Geochim. Cosmochim. Acta*, **53**, 1577–1581.

MURAT A. & GOT H. (2000). - Organic carbon variations of the eastern Mediterranean Holocene sapropel: a key for understanding formation processes. - *Palaeogeogr. Palaeoclimatol. Palaeoecol*., **158**, 241–257.

OLAUSSON E. (1961). - Studies of deep-sea cores. - *Reports of the Swedish Deep Sea Expedition 1947–1948*, **8**, 353–391.

ORCUTT B. N., SYLVAN J. B., KNAB N. J. & EDWARDS K. J. (2011). - Microbial ecology of the dark ocean above, at, and below the seafloor. - *Microbiol. Mol. Biol. Rev.*, **75**, 361–422.

PAILLARD D., LABEYRIE L. & YIOU P. (1996). - Macintosh Program performs time-series analysis. – *Eos,* Trans. Am. Geophys.Union, **77**, 39, 379–379.

PARKES R.J., CRAGG B., ROUSSEL E., WEBSTER G., WEIGHTMAN A. & SASS H. (2014). – A review of prokaryotic populations and processes in sub-seafloor sediments, including biosphere: geosphere interactions. - *Mar. Geol*., **352**, 409-425.

PEDERSEN T. & PRICE N. (1980). - The geochemistry of iodine and bromine in sediments of the Panama Basin. - *J. Mar. Res.,* **38**, 397–411.

PETIT S., CAILLAUD J., RIGHI, D. & MADEJOVÁ J. (2002). - Characterization and crystal chemistry of an Fer-rich montmorillonite from Ölberg, Germany. - *Clay Minerals,* **37**, 2, 283-297.

PETIT S. & DECARREAU A. (1990). - Hydrothermal (200 degrees C) synthesis and crystal chemistry of iron-rich kaolinites. - *Clay Minerals*, **25**, 2, 141-160.

PRICE N. B., CALVERT S. E. & JONES P. G. W. (1970). - The distribution of iodine and bromine in the sediments of the South Western Barents Sea. - *Mar. Res.***,** **28,** 22-34.

PRICE N. B. & CALVERT S. (1977). - The contrasting geochemical behaviours of iodine and bromine in recent sediments from the Namibian shelf. - *Geochim. Cosmochim. Acta*, **41**, 1769-1775.

PRYOR W. A. (1975). - Biogenic sedimentation and alternation of argillaceous sediments in shallow marine environments. - *Geological Society of America Bulletin*, **86**, 1244-1254.

R DEVELOPMENT CORE TEAM. (2013). - R: a Language and Environment for Statistical Computing. 3-900051-07-0 *R Foundation for Statistical Computing*, Vienna, Austria, URL ⟨http://www.R-project.org/⟩.

RICHTER T.O., VAN DER GAAST S., KOSTER B., VAARS A., GIELES R., DE STIGTER H.C., DE HAAS H. & VAN WEERING T.C.E. (2006). - The Avaatech XRF Core Scanner: technical description and applications to NE Atlantic sediments. - *Geological Society London, Special Publication*, **267**, 39-50.

RICKER W.E. (1973). – Linear regressions in fishery research. - *J. De. l'Off. Des. Rech. sur Les. Pêcheries Du. Can.,* **30**, 3,409–434.

ROHLING E.J. (1994). - Review and new aspects concerning the formation of Mediterranean sapropels. - *Mar. Geol.,* **122**, 1–28.

ROHLING E.J., MARINOA G. & GRANT K.M. (2015). - Mediterranean climate and oceanography, and the periodic development of anoxic events (sapropels). - *Earth-Science Reviews*, **143**, 62–97.

ROSSIGNOL-STRICK M. (1985). - Mediterranean Quaternary sapropels, an immediate response of the African monsoon to variations of insolation. - *Palaeogeogr. Palaeoclimatol. Palaeoecol*., **49**, 237–263.

SCHILMAN B., ALMOGI-LABIN A., BAR-MATTHEWS M., LABEYRIE, L., PETERNE M. & LUZ, B. (2001). - Long- and short-term carbon fluctuations in the eastern Mediterranean during the late Holocene. – *Geology*, **29**, 12, 1099–1102.

SOKAL R.R. & ROHLF F.J. (2012). - Biometry: The Principles and Practice of Statistics. – *in:* W. H. Freeman and Co Eds, Biological Research*,* 4th edition*.,* New York*,* 937p.

STANLEY, D. J., NIR, Y., & GALILI, E. (1998). - Clay mineral distributions to interpret Nile cell provenance and dispersal: III. Offshore margin between Nile delta and northern Israel. - *Journal of coastal Research*, **14**, 196-217.

STEFANELLI S., CAPOTONDI L. & CIARANFI N. (2005). – Foraminiferal record and environmental changes during the deposition of the Early-Middle Pleistocene sapropels in southern Italy. – *Palaeogeogr. Palaeoclimatol. Palaeoecol*., **216**, 27-52.

SURDAM R. C., DUNN T. L., HEATHER H.P. & MACGOWAN, D.B. (1989). - Integrated diagenetic modelling; a process orientated approach for clastic systems. *Annual Reviews of Earth and Planetary Science Letters*, **15**, 141-170.

TENHAVEN H. L., DELEEUW J. W., SCHENCK P. A. & KLAVER G. T. (1988). - Geochemistry of Mediterranean sediments—Bromine/organic carbon and uranium/organic carbon ratios as indicators for different sources of input and post-depositional oxidation, respectively. - *Org. Geochem*., **13**, 1–3, 255–261.

TJALLINGII R., RÖHL U., KÖLLING M. & BICKERT T. (2007). - Influence of the water content on X-ray fluorescence core-scanning measurements in soft marine sediments. - *Geochem. Geophys. Geosyst*., **8**, Q02004.

TISSOT B.P. & WELTE D.H. (1984). - Petroleum Formation and Occurrence. - 2nd. ed. Springer, Heidelberg, 601 p.

TRIBOVILLARD N., BOUT-ROUMAZEILLES V., SIONNEAU T., MONTERO-SERRANO J.C., RIBOULLEAU A. & BAUDIN F. (2009). - Organic-matter preservation and accumulation in an anoxic setting: the Orca Basin, Gulf of Mexico. *Comptes Rendus Geosciences*, **341**, 1-9.

UPSTILL-GODDARD R. C. & ELDERFIELD H. (1988). - The role of diagenesis in the estuarine budgets of iodine and bromine. - *Cont. Shelf Res.,* **8**, 405–430.

VETÖ I., HETÉNYI M., DEMÉNY A. & HERTELENDI E. (1994). - Hydrogen index as reflecting intensity of sulphidic diagenesis in non-bioturbated, shaly sediments. – *Org. Geochem.,* **22**, 299–310.

WANG P. X., TIAN J. & LOURENS L. J. (2010). - Obscuring of long eccentricity cyclicity in Pleistocene oceanic carbon isotope records. - *Earth and Planetary Science Letters*, **290**, 3-4, 319-330.

WORDEN R.H. & BURLEY S.D. (2003). - Sandstone diagenesis: the evolution from sand to stone. - *In:* S.D. Burley & R.H. Worden (Eds.), Clastic Diagenesis: Recent and Ancient, International Association of Sedimentologists, **4**, 3–44.

WORDEN R. H. & MORAD S. (2003). - Clay minerals in sandstones: controls on formation, distribution and evolution. - *In:* R.H. Worden & S. Morad (Eds.), Clay mineral cements in Sandstones. Blackwell Publishing, 3-41.

ZIEGLER M., JILBERT T., DE LANGE G. J., LOURENS L. J. & REICHART G.-J. (2008). - Bromine counts from XRF scanning as an estimate of the marine organic carbon content of sediment cores. - *G-cubed*, **9**, Q05009.

## Figure captions

Figure 1: Morphobathymetric map of the Nile margin and location of the studied core MD04 2723.

Figure 2: Core MD04 2723 data evolution with age: lithology, isotopic stratigraphy, Marine Isotopic Stages (MIS), Ca, BrTot, TOC and Sm%.

Figure 3: Modified van Krevelen diagram showing the sapropel results (N=20) with indications of the sapropel number and TOC content in %.

Figure 4: The relationship between TOC and solid-phase bromine. Bromine data values below the detection limit (5 ppm) were nullifying. Black dots: S5 sequence, Black squares: S28 sequence, Black dash: other sequences.

Figure 5: Evolution of the BrOrg/TOC ratio with age by sapropelic sequence.

Time is obviously a factor in BrOrg variability. The evolution of the slope (or ratio of BrOrg to TOC) with age indicates a loss of BrOrg of approximately 50% in 1.1 million years.

Figure 6: Evolution of BrOrg with age by TOC range. Red crosses: <0.5%, purple dots: 1.5-2.3%, blue triangles: 2.3-3% and green squares: 4.0-6.5%.

Figure 7: XRD patterns of the clay material extracted from sample MD04 2723 – 1 – 48. Diffractograms of the oriented preparations of the less than 2 µm fraction size acquired in air-dried conditions (A.D.) and after saturation with ethylene glycol.

Figure 8: Aspect of the smectitic material in the middle part of the S5 sapropelic horizon (section 6, 22.5-23.5 cm): (a) SEM observation, an intimate mixture of clay and carbonaceous particles in the bulk material; (b) flakes of smectite particles

deposited onto a glass slide; (c) HRTEM image of the individual crystallites of the smectite tactoids.

Figure 9: Decomposition of the near-infrared spectra of samples in which the clay material is composed of (a) 75% smectite–25% kaolinite and (b) 90% smectite–10% kaolinite. See Herbert et al., 2015 for more details on the method of quantification of Sm%.

Figure 10: Main results through time, solid-phase organic bromine evolution as a function of the TOC range (each straight line corresponds to a different debromination rate), and relative stability of the detrital montmorillonite supply.

Figures

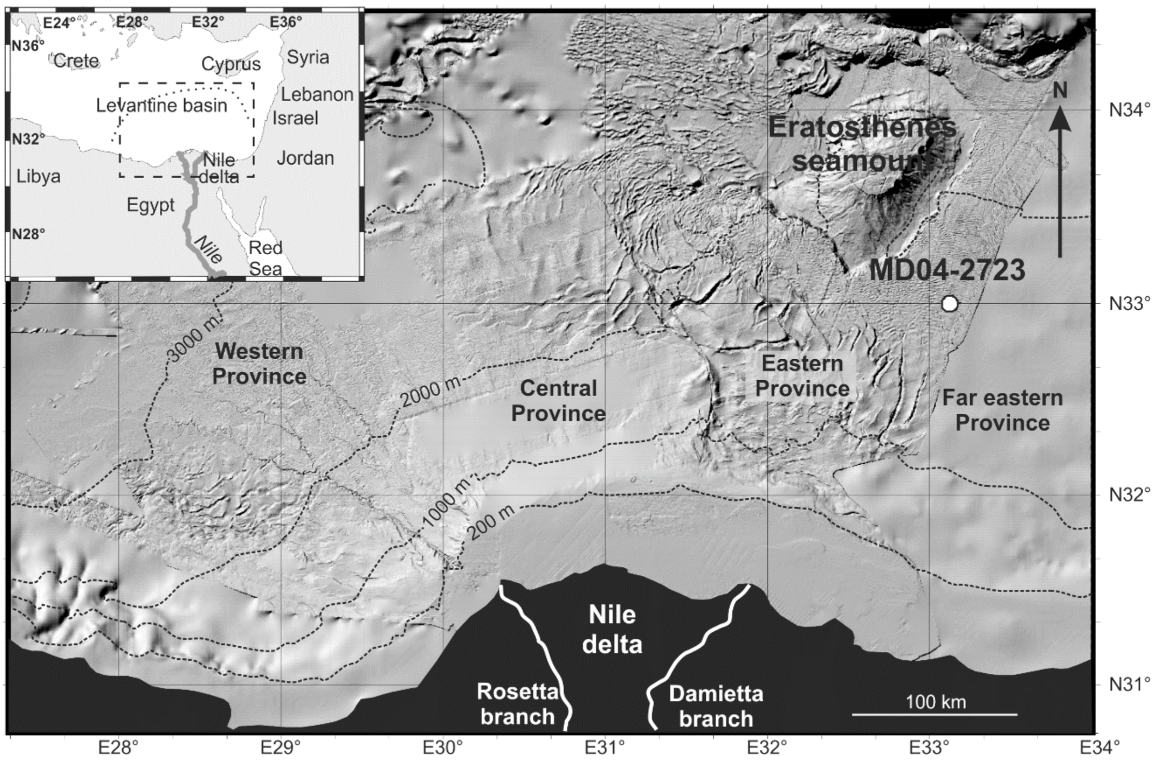

Figure 1

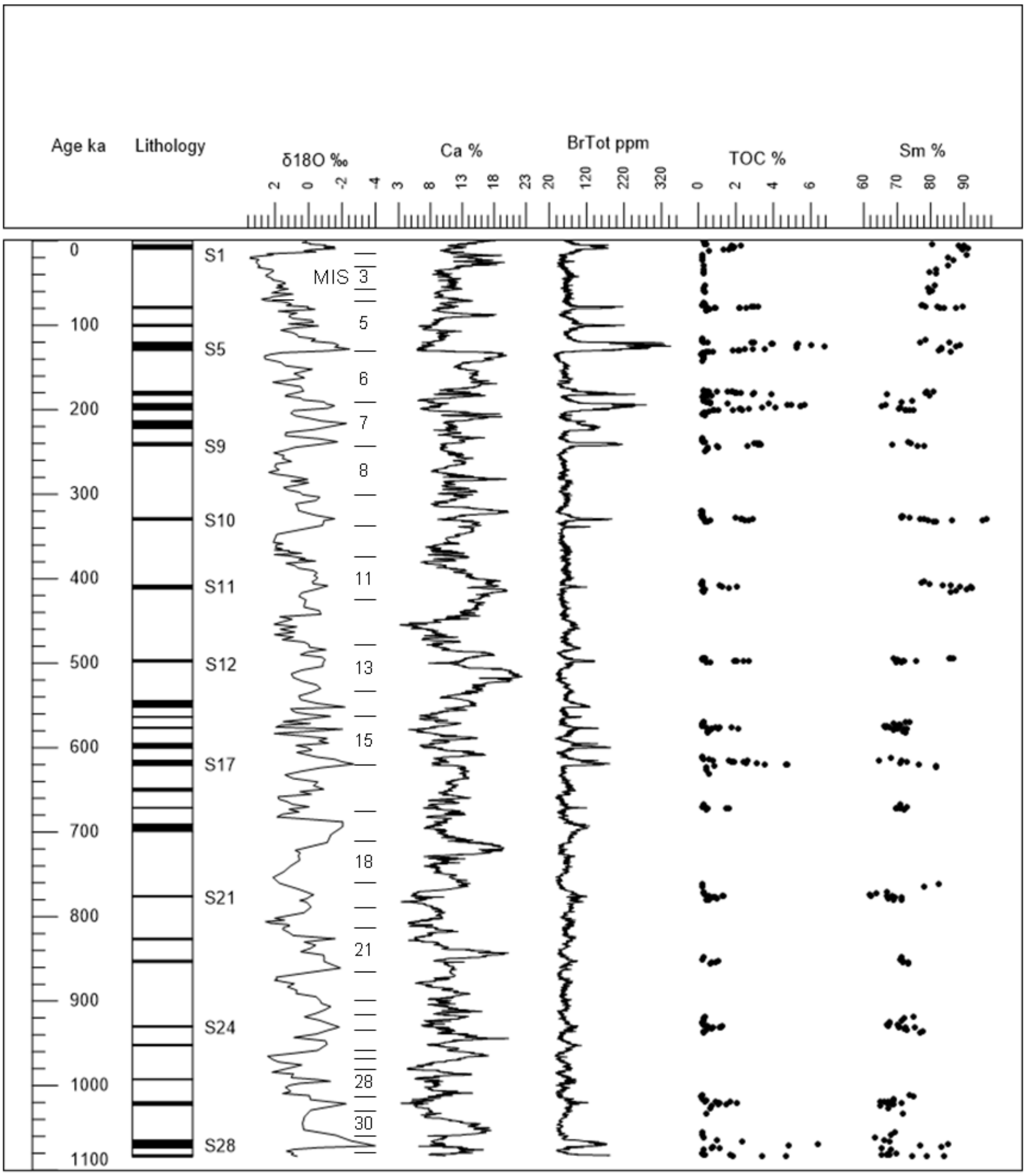
Age ka
Lithology
δ18O ‰
2
0
-2
-4
Ca %
3
8
13
18
23
BrTot ppm
20
120
220
320
TOC %
0
2
4
6
Sm %
60
70
80
90
0
100
200
300
400
500
600
700
800
900
1000
1100
S1
S5
S9
S10
S11
S12
S17
S21
S24
S28
MIS
3
5
6
7
8
11
13
15
18
21
28
30

Figure 2

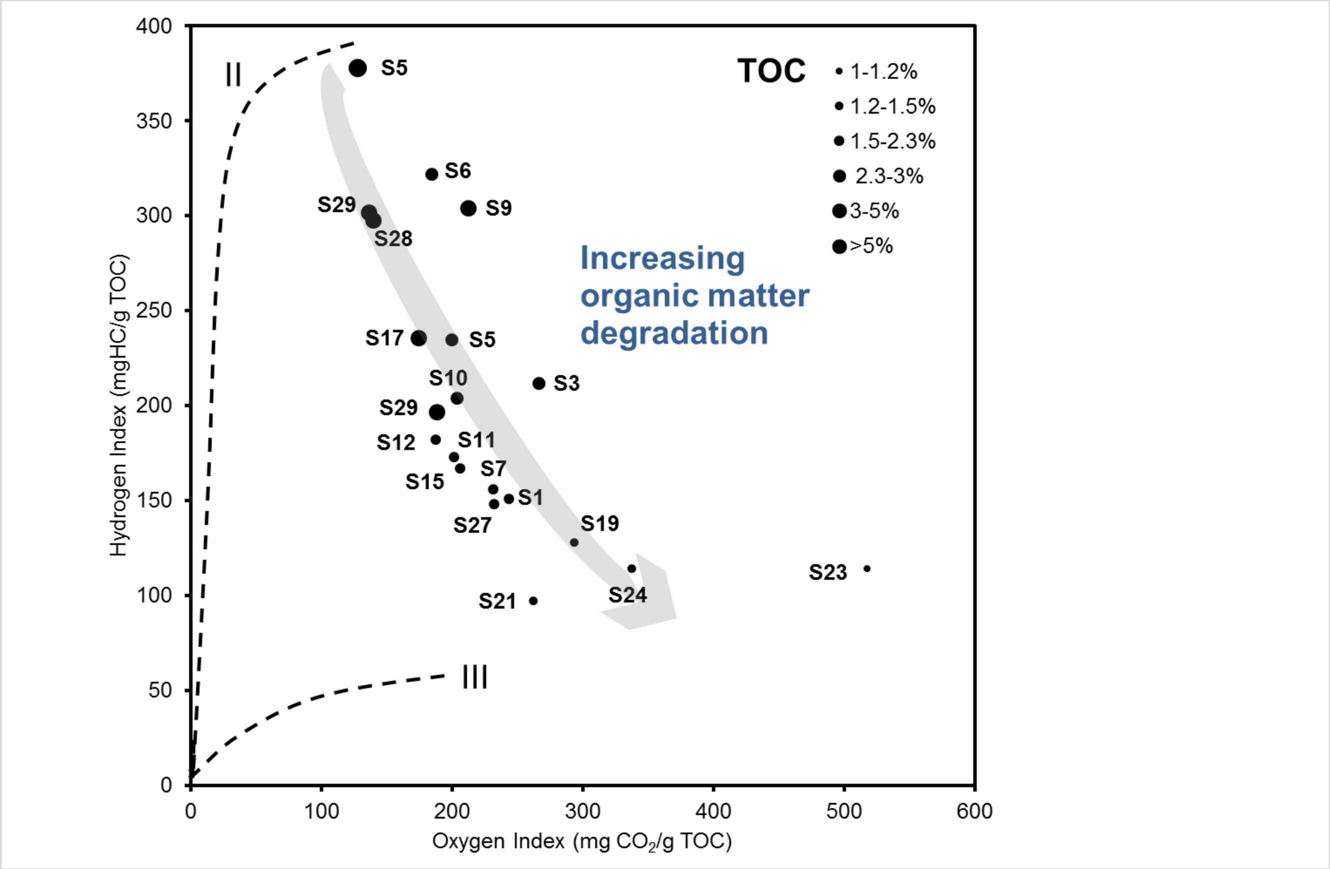
400
350
300
250
200
150
100
50
0
Hydrogen Index (mgHC/g TOC)
0
100
200
300
400
500
600
Oxygen Index (mg CO$_2$/g TOC)
II
III
TOC
• 1-1.2%
• 1.2-1.5%
• 1.5-2.3%
● 2.3-3%
● 3-5%
● >5%
Increasing organic matter degradation
S5
S6
S29
S9
S28
S17
S5
S10
S3
S29
S12
S11
S7
S15
S1
S27
S19
S23
S24
S21

Figure 3

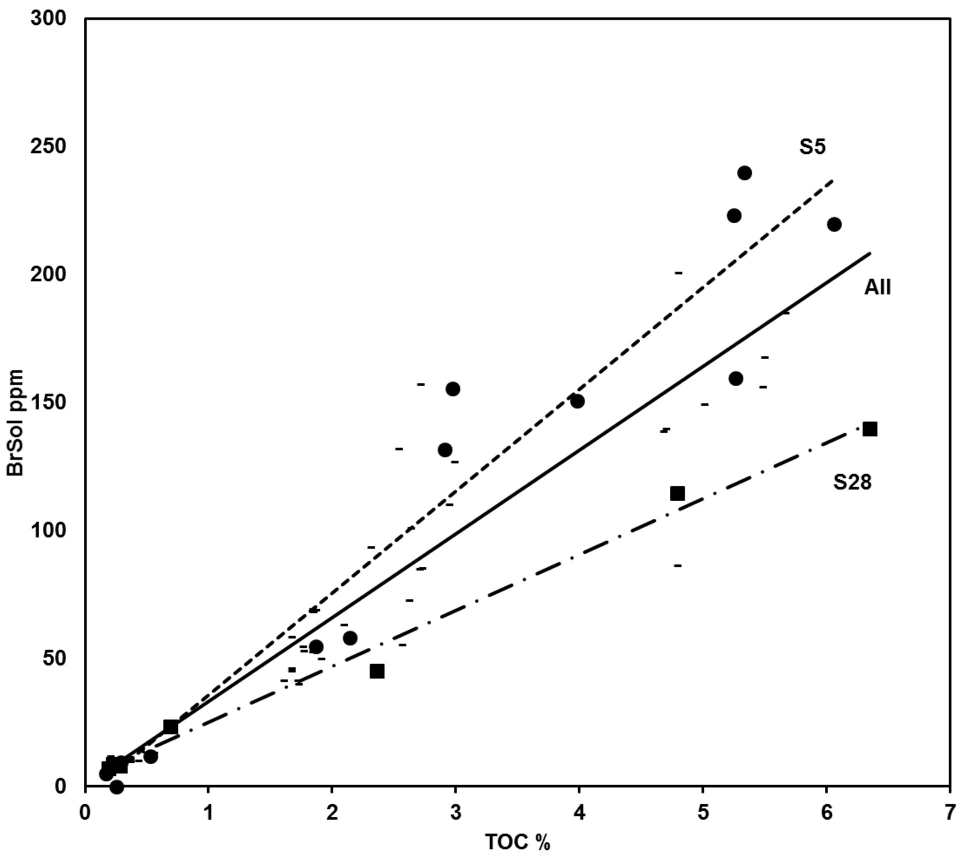

1003

1004 Figure 4

1005

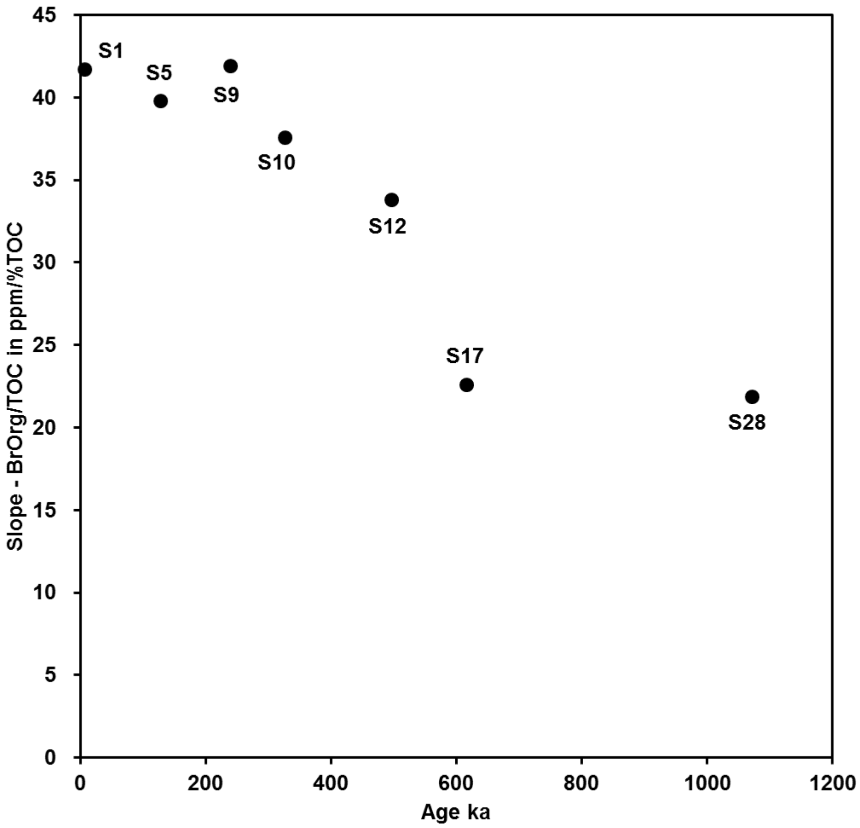

S1
S5
S9
S10
S12
S17
S28
Slope - BrOrg/TOC in ppm/%TOC
Age ka
0
5
10
15
20
25
30
35
40
45
0
200
400
600
800
1000
1200

Figure 5

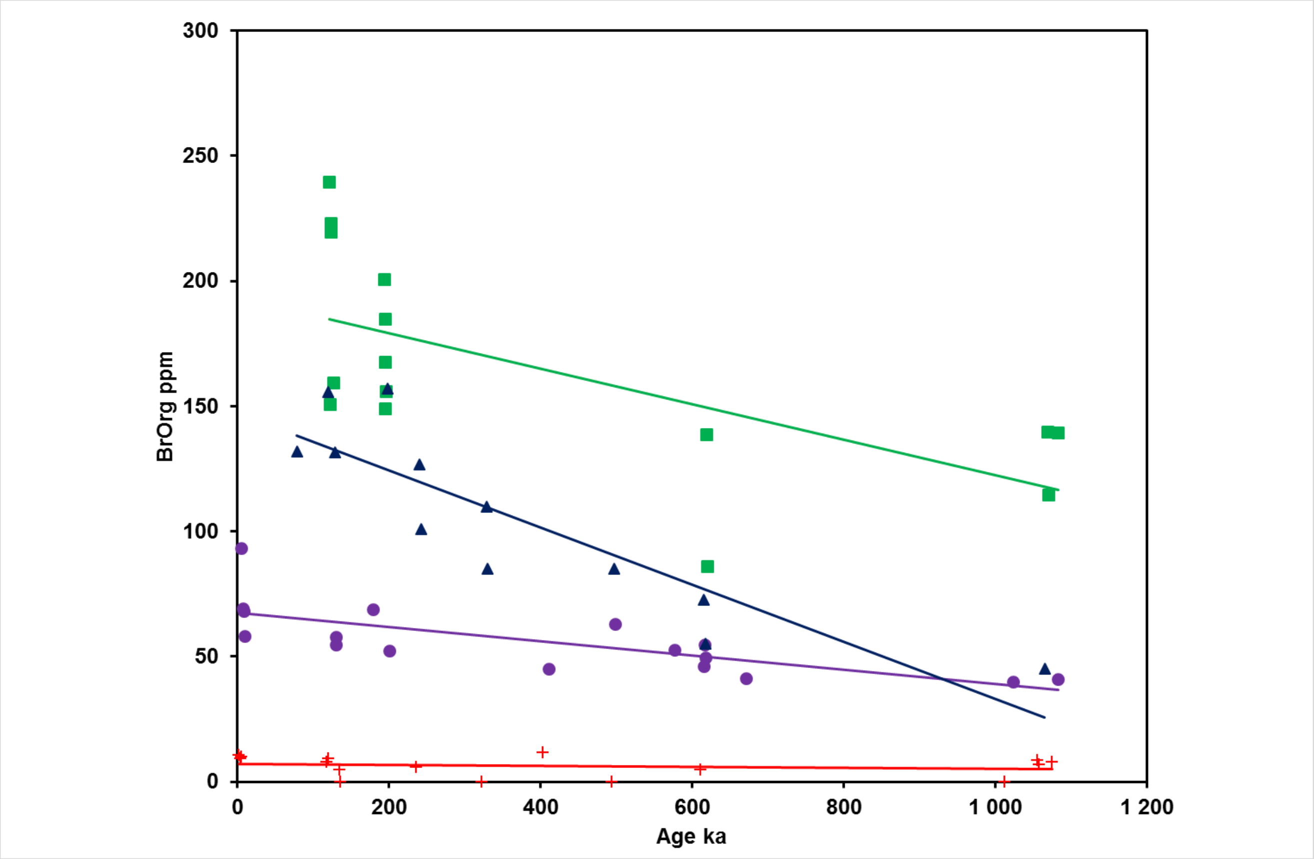
300
250
200
150
100
50
0
BrOrg ppm
0
200
400
600
800
1 000
1 200
Age ka

Figure 6

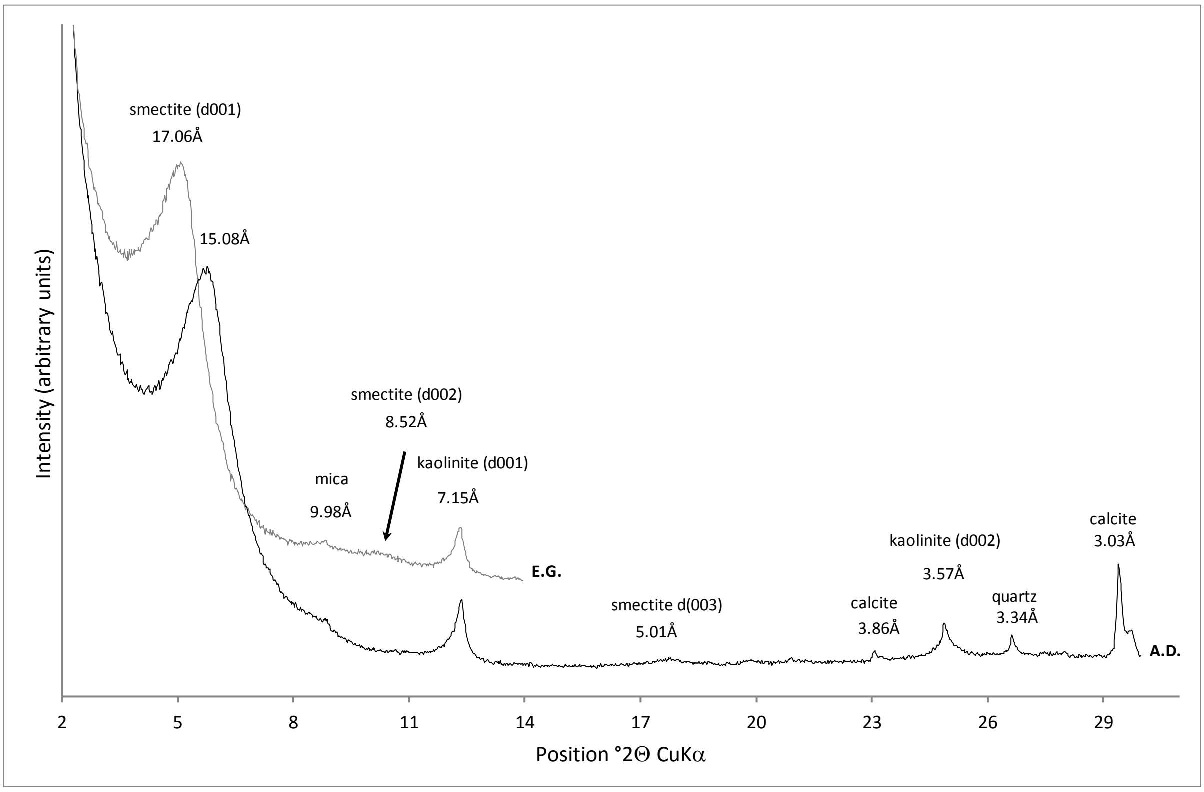
smectite (d001)
17.06Å
15.08Å
Intensity (arbitrary units)
smectite (d002)
8.52Å
mica
9.98Å
kaolinite (d001)
7.15Å
E.G.
smectite d(003)
5.01Å
calcite
3.86Å
kaolinite (d002)
3.57Å
quartz
3.34Å
calcite
3.03Å
A.D.
2
5
8
11
14
17
20
23
26
29
Position °2Θ CuKα

Figure 7

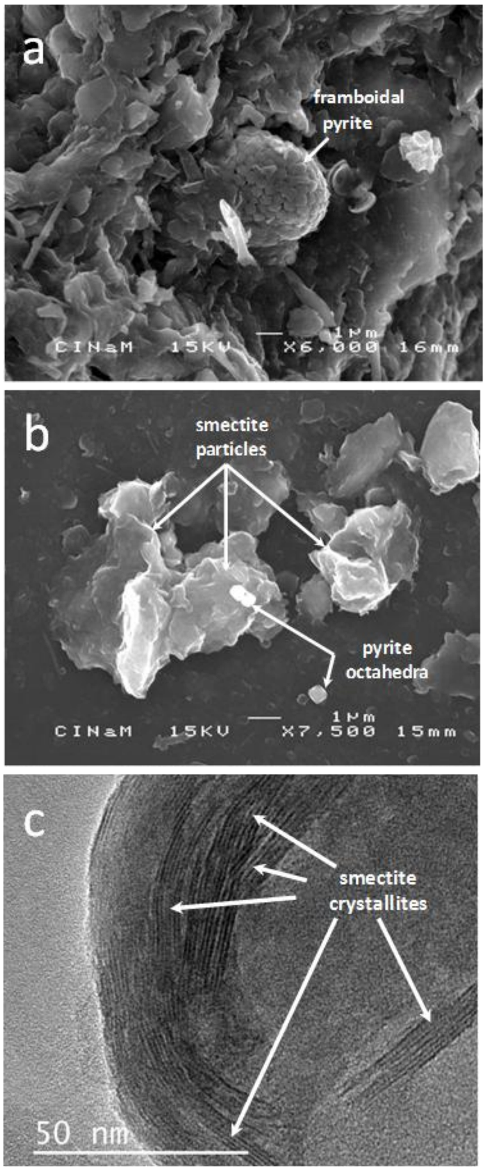
a
framboidal pyrite
CINaM 15KV 1µm X6,000 16mm
b
smectite particles
pyrite octahedra
CINaM 15KV 1µm X7,500 15mm
c
smectite crystallites
50 nm

Figure 8

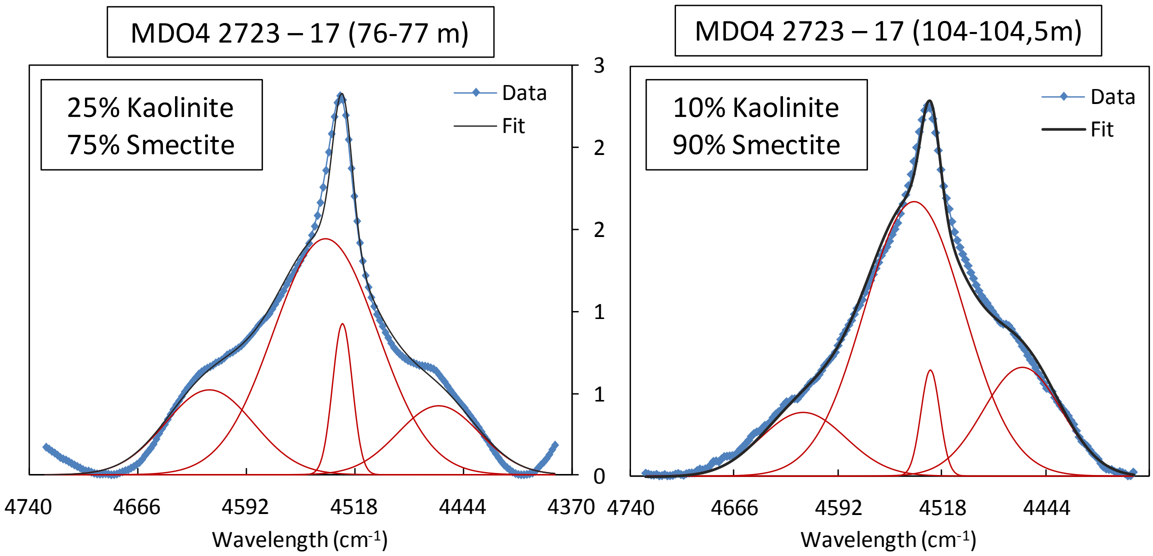
MDO4 2723 – 17 (76-77 m)
25% Kaolinite
75% Smectite
Data
Fit
MDO4 2723 – 17 (104-104,5m)
10% Kaolinite
90% Smectite
Data
Fit
3
2
2
1
1
0
4740
4666
4592
4518
4444
4370
4740
4666
4592
4518
4444
Wavelength (cm-1)
Wavelength (cm-1)

Figure 9

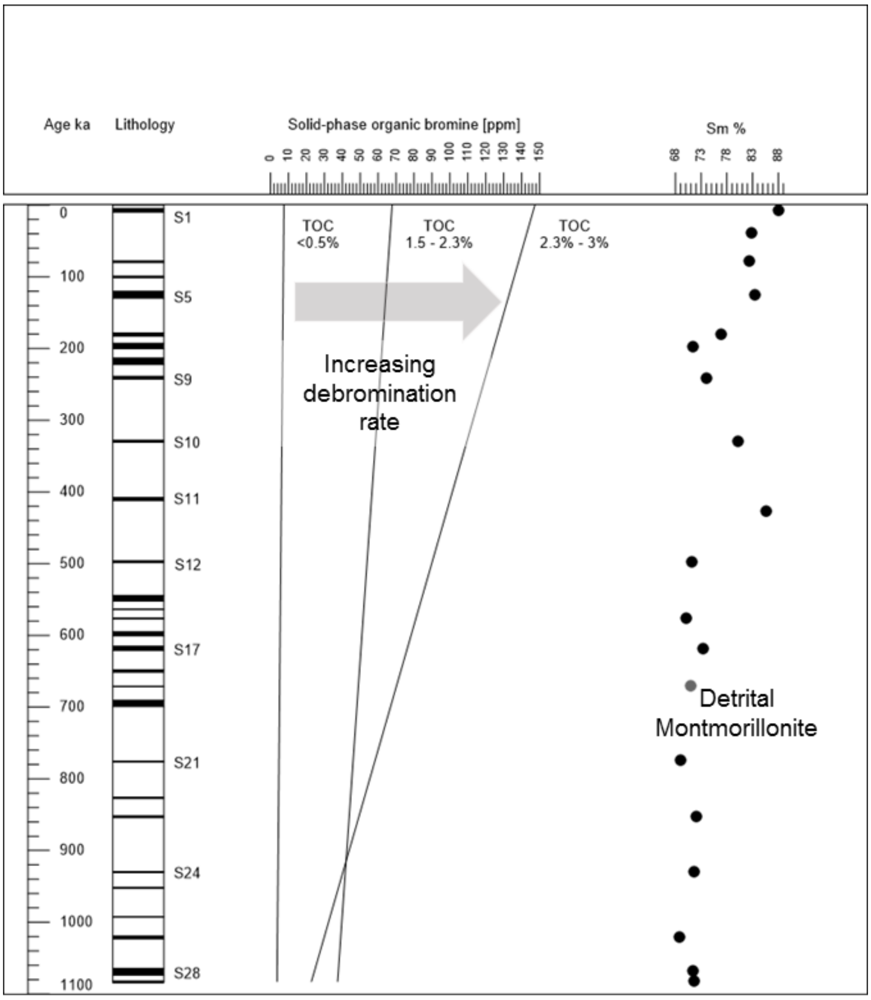
Age ka
Lithology
Solid-phase organic bromine [ppm]
0
10
20
30
40
50
60
70
80
90
100
110
120
130
140
150
Sm %
68
73
78
83
88
0
100
200
300
400
500
600
700
800
900
1000
1100
S1
S5
S9
S10
S11
S12
S17
S21
S24
S28
TOC <0.5%
TOC 1.5 - 2.3%
TOC 2.3% - 3%
Increasing debromination rate
Detrital Montmorillonite

Figure 10

## Table captions

Table 1: Statistical results of the regression analysis of the TOC-BrOrg relationship. $p > 0.05$ is non significant (NS), $p$ between 0.05 and 0.01 is significant (S), $p$ between 0.01 and 0.001 is highly significant (HS), and $p < 0.001$ is very highly significant (VHS). The slope corresponds to the ratio of BrOrg to TOC in ppm/%TOC.

Table 2: Evolution of BrOrg with age by TOC range. Statistical results: $p > 0.05$ is non significant (NS), $p$ between 0.05 and 0.01 is significant (S), $p$ between 0.01 and 0.001 is highly significant (HS), and $p < 0.001$ is very highly significant (VHS).

Table 3: Representative structural formulas of smectite particles analyzed by TEM-EDX (1 and 2) and SEM-EDX(3-5). Number of ions calculated on the basis of 11 oxygens (Fe arbitrarily considered as $Fe^{3+}$). Int. ch: interlayer charge.

# Tables

| Sequence | Age [ka] | N | r | $r^2$ | *p* -value | Slope | Intercept |
|---|---|---|---|---|---|---|---|
| All data | | 63 | 0.922 | 0.851 | VHS | 32.8 | 0.44 |
| S1 | 6.13 | 8 | 0.996 | 0.993 | VHS | 41.7 | -6.83 |
| S5 | 127.47 | 14 | 0.968 | 0.937 | VHS | 39.8 | -3.90 |
| S9 | 238.94 | 3 | 0.996 | 0.992 | NS | 41.9 | -2.72 |
| S10 | 326.65 | 3 | 0.991 | 0.982 | NS | 37.6 | -7.51 |
| S12 | 495.89 | 3 | 0.999 | 0.999 | S | 33.8 | -6.86 |
| S17 | 615.48 | 8 | 0.909 | 0.825 | HS | 22.6 | 7.06 |
| S28 | 1071.57 | 7 | 0.995 | 0.990 | VHS | 21.9 | 3.13 |

Table 1

| TOC range | Mean TOC | N | r | $r^2$ | *p* -value | Slope | Intercept | % of loss BrOrg in 1 m.y. | Debromination rate [µmolBrOrg $molC^{-1}$ $y^{-1}$] |
|---|---|---|---|---|---|---|---|---|---|
| < 0.5% | 0.24 | 16 | -0.171 | 0.029 | NS | -0.002 | 6.92 | NS | NS |
| 1.5 - 2.3 % | 1.83 | 17 | -0.736 | 0.542 | HS | -0.028 | 67.53 | 41 | $2.3\ 10^{-4}$ |
| 2.3 - 3.0 % | 2.73 | 12 | -0.878 | 0.771 | HS | -0.115 | 147.46 | 78 | $6.3\ 10^{-4}$ |
| 4.55 - 5.4% | 4.95 | 9 | -0.688 | 0.473 | S | -0.087 | 201.34 | 43 | $2.6\ 10^{-4}$ |
| 5.4 - 6.5% | 5.80 | 5 | -0.671 | 0.450 | NS | -0.051 | 192.07 | NS | NS |
| 4.0 - 6.5 % | 5.17 | 15 | -0.640 | 0.410 | S | -0.071 | 193.31 | 37 | $2.0\ 10^{-4}$ |

Table 2

|  | 1 | 2 | 3 | 4 | 5 |
|---|---|---|---|---|---|
| Si | 3.97 | 3.83 | 3.91 | 3.91 | 3.84 |
| Al$^{IV}$ | 0.03 | 0.17 | 0.09 | 0.09 | 0.16 |
| Al$^{VI}$ | 1.24 | 1.14 | 1.35 | 0.88 | 1.45 |
| Fe$^{3+}$ | 0.31 | 0.26 | 0.28 | 0.53 | 0.26 |
| Mg | 0.53 | 0.65 | 0.37 | 0.59 | 0.29 |
| Ca | 0.09 | 0.17 | 0.03 | 0.05 | 0.14 |
| Na | 0.10 | 0.17 | 0.25 | 0.31 | 0.12 |
| K | 0.06 | 0.14 | 0.14 | 0.26 | 0.07 |
| Int. Ch. | 0.35 | 0.65 | 0.45 | 0.67 | 0.47 |

Table 3